







Cite this: *Sens. Diagn.*, 2023, 2, 1574

Efficient detection of bilirubin in human serum through a displacement approach†

Nancy Singla,  Manzoor Ahmad,  Vishal Mahajan, Prabhpreet Singh  and Subodh Kumar *

The present study provides, for the first time, a method for the fluorescence “Turn ON” quantification of bilirubin (BR) in human serum through a displacement approach. The fluorescent probe THYQ exhibited a 55-fold increase in fluorescence intensity at 555 nm with HSA. The green fluorescent THYQ–HSA complex was highly selective towards bilirubin (BR) (subdomain IB) and exhibited >90% fluorescence quenching ($\log \beta = 4.83 \pm 0.12$) through the displacement of THYQ, whereas the subdomain IIA and subdomain IIIA selective drugs warfarin and ibuprofen did not displace THYQ. The non-fluorescent BR–HSA complex displayed a linear increase in fluorescence with THYQ ($\log \beta = 4.81 \pm 0.13$) to form THYQ–HSA complex. The slope of titration of BR–HSA with THYQ was linearly dependent on [bilirubin] in HSA, thus enabling the fluorescence-based detection of bilirubin below normal (0.7 mg dL^{-1} , $12 \text{ }\mu\text{M}$) to hyperbilirubinemia conditions (12.6 mg dL^{-1} , $216 \text{ }\mu\text{M}$), with the results in good agreement with the clinical findings. The LOD for the detection of BR was 0.004 mg dL^{-1} (68 nM).

Received 22nd June 2023,
Accepted 21st September 2023

DOI: 10.1039/d3sd00157a

rsc.li/sensors

1. Introduction

The levels of bilirubin (BR) need to be maintained for the wellbeing of humans and thus the monitoring of BR is critical, and has attracted increasing attention as the number of deaths due to hyperbilirubinemia has doubled over the past two decades.¹ Its increased levels, such as in jaundice, are associated with acute and chronic health burden, while low levels have been linked to iron deficiency (anaemia) and coronary artery diseases.^{2,3} The normal concentration of bilirubin in adult serum lies between 0.2 and 1.2 mg dL^{-1} . In the condition of hyperbilirubinemia, it can go up to 9.9 mg dL^{-1} ($170 \text{ }\mu\text{M}$) in an adult and even to $>24.8 \text{ mg dL}^{-1}$ ($425 \text{ }\mu\text{M}$) under critical neonatal and other hyperbilirubinemia conditions.

At present, the clinical quantification of bilirubin depends on the diazotization reaction between bilirubin and sulfanilic acid, which was devised more than 100 years ago.⁴ However, the complexity of the chemical reactions and inhomogeneity of biological samples make this procedure unreliable.⁵ A fluorescence-based assay depending on clean chemical events could be expected to be more advantageous.

Several fluorescence methods, using carbon dots,^{6–8} metal nanoclusters,⁹ MOFs,^{10,11} organic molecules,^{12–17} have been developed for the detection of bilirubin. However, these are limited due to the “Turn OFF” signal and poor sensitivity and dependence on a spiking method for clinical detection. Recently reported coumarin-based *N*-oxide- Fe^{3+} mixtures have revealed “Turn ON” fluorescence in the presence of bilirubin owing to the deoxygenation process by the *in situ* generated Fe^{2+} (ref. 16 and 17) and have been tested and even used for the detection of bilirubin from human serum. In another approach, in non-fluorescent resorcinol-sucrose CDs and Cu^{2+} complex, the competitive binding of Cu^{2+} with bilirubin released the fluorescence of the CDs.⁸ Most of these methods for the detection of bilirubin from human serum have a myriad of limitations and in general have low sensitivity and depend on a spiking approach.

The human serum albumin (HSA) concentration in human serum is between 500 and $700 \text{ }\mu\text{M}$ and bilirubin remains bound to it with high affinity, and this formed BR–HSA complex acts as a buffer to prevent the transfer of bilirubin from blood to the tissues and thus plays a critical role in impairing the development of bilirubin encephalopathy.^{18,19} In the literature, numerous probes for the fluorescence-based detection of HSA have been reported, but most of these fluorescence probes bind at Site I and Site II, *i.e.* the respective warfarin and ibuprofen sites of HSA. We envisaged that a fluorescent probe (i) that could selectively bind at Site IB – the bilirubin site of HSA – and (ii) that has a binding constant similar to that of bilirubin with HSA so that it could

Department of Chemistry, Centre for Advanced Studies, Guru Nanak Dev University, Amritsar, Punjab, India. E-mail: subodh_gndu@yahoo.co.in, subodh.chem@gndu.ac.in

† Electronic supplementary information (ESI) available. See DOI: <https://doi.org/10.1039/d3sd00157a>



displace BR from the BR-HSA complex, with a resultant change in fluorescence intensity (FI), could be useful for the detection of bilirubin present in human serum without altering the physiological conditions.

The displacement approach is based on the competition between a probe and the analyte of interest for the binding site. Upon the addition of the analyte, the probe is displaced from the binding pocket, causing a signal change, such as in UV or fluorescence. This approach can enable the easy and real-time determination of an analyte without harming any of the substrate,²⁰ which is often not achieved by traditional chemosensors. Recently reported Site IB selective fluorescent probes, however, lack the reversible displacement of BR and the probe with HSA under physiological conditions.²¹

Now, we report a fluorescent probe THYQ that can enable the highly selective displacement of bilirubin from THYQ-HSA complex under physiological concentrations of HSA and that could be applied for the detection of bilirubin from human serum. The THYQ probe displayed a 55-fold increase in fluorescence intensity at 555 nm with HSA. The fluorescent THYQ-HSA complex was highly selective towards bilirubin and revealed >90% fluorescence quenching with $\log\beta = 4.83 \pm 0.12$, while the non-fluorescent BR-HSA displayed a linear increase in fluorescence with THYQ with $\log\beta = 4.81 \pm 0.13$. All the experiments for the detection of bilirubin (BR) were performed in HEPES buffer with $\sim 500 \mu\text{M}$ HSA. The slope of titration of the BR-HSA complex with THYQ was found to be linearly dependent on [BR], enabling the fluorescence-based detection of BR below normal (0.7 mg dL^{-1} , $12 \mu\text{M}$) to hyperbilirubinemia conditions (12.6 mg dL^{-1} , $216 \mu\text{M}$). The LOD for the detection of BR was 0.004 mg dL^{-1} (68 nM).

2. Experimental

2.1. Materials and methods

All chemicals and solvents were purchased from Aldrich and Spectrochem India, and were used without any purification. The organic solvents, including DMSO, DMF, and THF, were of HPLC grade. The ^1H and ^{13}C NMR spectra were recorded on a JEOL 400 MHz FT NMR machine using CDCl_3 as solvent and tetramethylsilane (TMS) as the internal standard. The chemical shift values of the peaks were recorded in ppm relative to TMS as the internal standard, with the coupling constant J in Hz, and multiplicity also noted (s = singlet, d = doublet, t = triplet, m = multiplet). High-resolution mass spectra were recorded on an Agilent 6520 Q-TOF mass spectrometer with the Agilent 1200 HPLC system. Deionized water was used throughout the experiments for preparing all solutions and obtained using an ultra UV/UF Rions lab water system ultra 370 series. UV-visible studies were performed on a Shimadzu UV-2450 instrument using a slit width of 1.0 nm and matched quartz cell with a 1 cm path length, thermo stated at $25.0 \pm 0.1^\circ\text{C}$. The fluorescence spectra were recorded on a Horiba Fluorolog-3 spectrophotometer with a quartz cuvette of 1 cm path length. DLS experiments were

performed at $25.0 \pm 0.1^\circ\text{C}$ by using a zeta sizer instrument (Nano ZS, Malvern LTD, UK).

2.2. Synthesis

2.2.1. Synthesis of NCI-1. *N,N*-Dimethylacetophenone (10 mmol, 1.6 g) was dissolved in DMF (10 ml) in a 100 ml round-bottom flask and then cooled to 0°C . Then POCl_3 (30 mmol, 3 ml, 4.94 g) was added drop-wise maintaining the temperature between 0 – 5°C . The reaction mixture was stirred at this temperature for 3 h at room temperature (RT). When the reaction was completed (according to TLC monitoring), the reaction mixture was poured into crushed ice with stirring and the solution was neutralized with potassium carbonate to pH 6 by keeping the temperature below 5°C . The obtained red product separated was filtered and dried. The red solid was purified by silica gel column chromatography to give the desired product **NCI-1** (1.5 g, 71.4% yield). ^1H NMR (400 MHz, CDCl_3 , ppm): δ 10.13 (1H, d, $J = 7.2 \text{ Hz}$), 7.66 (2H, d, $J = 9.2 \text{ Hz}$), 6.65 (2H, d, $J = 9.2 \text{ Hz}$), 6.56 (1H, d, $J = 7.2 \text{ Hz}$), 3.05 (6H, s).

2.2.2. Synthesis of Th-Y. **NCI-1** was dissolved in 10 ml DMF, and a solution of Na_2S (5.5 mmol, 0.43 g) in H_2O was added and the resulting reaction mixture was stirred at 60°C 2 h. Then, an aqueous solution of chloroacetaldehyde (5.5 mmol, 0.431 g, 0.35 ml) was added and stirring was continued for 3 h. When the reaction was completed (according to TLC monitoring), K_2CO_3 (5.5 mmol, 0.76 g) was added and the solution was then cooled to RT. The precipitates were filtered off under a vacuum to obtain the desired product **Th-Y** (1.84 g, 80%). ^1H NMR (400 MHz, CDCl_3 , ppm): δ 9.82 (s, 1H), 7.67 (d, 1H, $J = 4.0 \text{ Hz}$), 7.57 (2H, d, $J = 8.8 \text{ Hz}$), 7.25 (1H, d, $J = 4.0 \text{ Hz}$), 6.72 (2H, d, $J = 12 \text{ Hz}$), 3.03 (6H, s).

2.2.3. Synthesis of THYQ. 2-Methylquinoline (1.12 mmol, 160 mg) and benzoyl chloride (0.56 mmol, 80 mg) were dissolved in DMF (10 ml). The reaction mixture was stirred at RT for 20 min. Then, **Th-Y** (0.56 mmol, 130 mg) was added and the reaction mixture was stirred at 160°C for 5 h. The reaction mixture was then cooled to RT and diluted with water (30 ml). The solid was separated out by filtrating under vacuum and was purified by column chromatography to obtain **THYQ** (0.6 g, 84% yield). ^1H NMR (400 MHz): δ = 3.00 (s, 6H), 6.73 (d, $J = 8.8 \text{ Hz}$, 2H), 7.10–7.17 (m, 3H), 7.42–7.51 (m, 1H), 7.52 (d, $J = 8.8 \text{ Hz}$, 2H), 7.57 (d, $J = 8.8 \text{ Hz}$, 1H), 7.69 (t, $J = 7.2 \text{ Hz}$, 1H), 7.76 (d, $J = 8.8 \text{ Hz}$, 1H), 7.81 (d, $J = 16 \text{ Hz}$, 1H), 8.05 (d, $J = 8.8 \text{ Hz}$, 1H), 8.09 (d, $J = 8.8 \text{ Hz}$, 1H); ^{13}C NMR (100 MHz): δ 40.4, 112.5, 119.5, 120.4, 121.5, 122.5, 125.9, 126.9, 127.2, 127.5, 127.9, 128.7, 129.1, 129.6, 129.7, 129.8, 136.3, 146.3, 150.4, 155.9. HRMS (EI) m/z calculated for $\text{C}_{23}\text{H}_{20}\text{N}_2\text{S}$ (M^+): 356.1347, found ($\text{M}^+ + 1$) 357.1418.

2.3. Preparation of the stock solutions

A stock solution of the fluorescent probe **THYQ** (1 mM) was prepared in THF and was further diluted for preparing solutions of the desired concentrations. For the preparation



of 10 μM solution, 30 μL of stock solution was added in to 3 ml of the desired solvent, like THF-HEPES mixture or HEPES buffer. Every time, only a freshly prepared stock solution of bilirubin was used and this was prepared in DMSO. All the proteins, amino acids, anions, and thiols were prepared by dissolving commercial reagents in Millipore double-distilled water.

2.4. Detection limit²²

The lowest detection limit was calculated from fluorescence studies. The standard deviation was calculated by measuring the fluorescence data of **THYQ** three times. The slope was calculated from the graph of the fluorescence intensity vs. the concentration of the analyte added. The lowest limit of detection (LOD) was determined by using the following equation:

$$\text{LOD} = 3\sigma/k$$

where σ is the standard deviation of the blank measurements, and k is the slope of the straight line from the intensity vs. concentration graph.

2.5. Quantum yield calculation²³

The quantum yield (Φ) of the solutions of **THYQ** was measured with an integrated sphere on an FL-1039A/40A machine by using the excitation wavelength at 420 nm.

2.6. Binding constants²⁴

In order to determine the formation of various stoichiometric complexes and their binding constants, the whole spectral data of the titration experiments were evaluated using the software SPECFIT-32. This software is able to perform a global analysis of the equilibrium and kinetic systems with a singular value of decomposition and using nonlinear-regression modelling by the Levenberg-Marquardt method. The program simulates the fluorescence data obtained experimentally. The stoichiometry of the species formed, distribution of species, and their association constants are determined through the fitted model.

2.7. Measurement of circular dichroism²⁵

The alterations in the secondary structure of HSA in the presence of **THYQ** were studied by measuring the circular dichroism (CD) on a BIO-Kine 32 MOS 500 spectrophotometer using a quartz cuvette of path length 1 cm at 0.25 nm data pitch intervals. All the CD spectra were taken in the wavelength range 200–250 nm. The concentration of HSA was 0.5 μM . The helicity content was calculated from the MRE values at 222 nm using the following equation:

$$\% \alpha\text{-helix} = \frac{-(\text{MRE}_{222} - 2340)}{30300} \times 100$$

$$\text{MRE}(\text{deg cm}^2 \text{ dmol}^{-1}) = \frac{\theta_{\text{obs}}}{C_p n l \times 10}$$

Here, the mean residue ellipticity (MRE) values were assessed from the recorded ellipticity values (θ_{obs} in mdeg at 222 nm) using the above equations, where n designates the number of amino acid residues (585 for HSA), and C_p and l are the molar concentration of HSA and the path length of the cell (here 1 cm), respectively.

2.8. DLS sample preparation

The solvents THF and HEPES buffer were separately filtered through a 0.02 μM filter to remove any suspended particles. The DLS samples were prepared by diluting the 30 μL of stock solution into 3 ml of either THF or deionized water or their mixture and then allowed to stand for 3 h so that the solutions became homogenous. For recording the DLS spectra, 1 ml of solution was taken into a glass cuvette of 1 cm path length and allowed to stand for 3 min before recording the spectra at 25 $^{\circ}\text{C}$. Five measurements of each sample were recorded and the mean of these are presented herein.

2.9. Collection of human blood serum samples for the quantification of bilirubin

The human blood serum samples were collected from Dr Gill Path's laboratory. The values of bilirubin (calculated by the diazo method) present in human serum were provided by the laboratory and are mentioned in Table 1 (section 5). Prior to the fluorescence analysis, all the samples were centrifuged at 7000 rpm for 10 min. The supernatant liquid obtained was used and stored immediately at 4 $^{\circ}\text{C}$. All the fluorescence measurements were carried out in a 1 ml quartz cuvette of 1 cm path length.

2.10. Determination of bilirubin in clinical samples

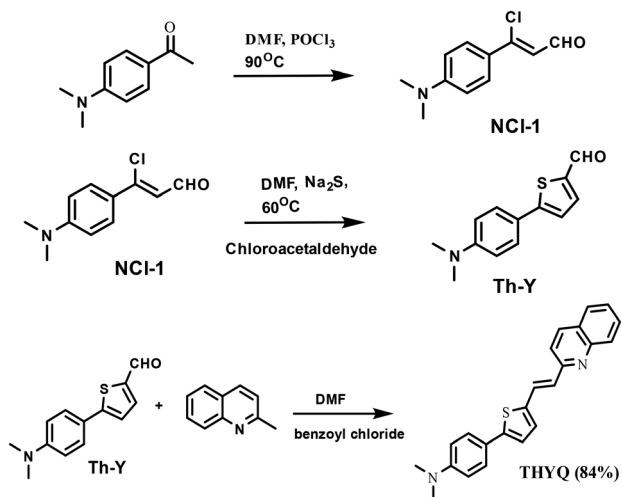
To the solutions of HSA (500 μM) and bilirubin (0, 10, 20, 40 μM) **THYQ** was added in varying amounts as 10, 20, 30, and 40 μM and the slope of the FI vs. [**THYQ**] graphs was determined. The plot of the slopes of these graphs vs. [bilirubin] was linear, and served as a calibration curve for the quantification of BR from the real samples. The real samples after diluting with HSA (500 μM) were titrated with **THYQ** (10, 20, and 40 μM) and the slopes were calculated. These slope values were then marked on the calibration curve and the corresponding BR concentration was noted.

3. Results and discussion

3.1. Synthesis and characterization of **THYQ**

NCl-1 was synthesized by Duff's reaction of *N,N*-dimethylacetophenone. The reaction of **NCl-1** with chloroacetaldehyde in DMF and Na_2S yielded **Th-Y** in an 80% yield. The reaction of **Th-Y** with 2-methylquinoline gave





Scheme 1 Synthetic schemes for the syntheses of NCI-1, Th-Y, and THYQ.

THYQ (Scheme 1) in an 84% yield; HRMS ($M + 1$) 357.1418 (spectral data ESI[†] Fig. S1–S5).

3.2. Photophysical behaviour of THYQ in the THF-HEPES buffer binary mixtures

Fluorescent probes for the recognition of HSA, in principle, may undergo aggregation-induced quenching in water and then, upon moving the probe in to the cavity of HSA, the combined effect of de-aggregation and the restriction in rotation results in a fluorescence enhancement. Therefore, as a first step, the optical behaviour of **THYQ** in THF-H₂O binary mixtures was investigated.

The UV-vis spectrum of **THYQ** (10 μM) in THF exhibited an absorption maximum at ~420 nm. The absorption of **THYQ** displayed only a small change in its ϵ value ($\epsilon = 26\,000 \pm 1200\text{ M}^{-1}\text{ cm}^{-1}$) upon increasing f_w (HEPES buffer) from 10% to 70% (Fig. 1A). The **THYQ** solution with f_w 80% showed a dramatic decrease in absorption to $7400\text{ M}^{-1}\text{ cm}^{-1}$ and its maximum was blue-shifted to 415 nm. Upon further increasing the f_w to 90% and 99.9%, the absorption value increased to $>10\,000\text{ M}^{-1}\text{ cm}^{-1}$ with the maximum at 410 nm and a shoulder at ~465 nm. The tail of the absorbance band was extended to 650 nm, pointing to Mie scattering by the aggregates of **THYQ** (Fig. 1A). This blue-shift in the absorbance maximum and decrease in the absorbance with increasing amounts of water suggests the formation of H aggregates.²⁶ The appearance of the Tyndall effect by striking a red laser beam to the solution of **THYQ** in 99.9% f_w further supports the existence of aggregates (see inset Fig. 1A).

The fluorescence spectrum of **THYQ** (10 μM, THF) (λ_{ex} 420 nm) showed the emission maximum at 562 nm. The solutions with increasing f_w (HEPES buffer) exhibited a gradual red-shift of their emission maxima reaching the largest value at 647 nm in THF-HEPES buffer mixture with 80% f_w , but upon further raising the f_w to $\geq 90\%$, a very weak fluorescence with the maximum reversed to

572 nm was noted. The red-shift in the emission maximum from 562 nm to 647 nm ($\sim \Delta 85\text{ nm}$) suggests a steady stabilization of the excited state of **THYQ** with increasing the amount of the water fraction and a decrease in the energy gap between the ground and excited states²⁷ (Fig. 1B and C). The inset in Fig. 1C shows the change in colour of the solutions of **THYQ** in THF-water binary mixtures under illumination of 365 nm light. The decrease in fluorescence intensity of **THYQ** with $f_w \geq 90\%$ suggests aggregation-induced emission quenching (AIEQ) occurred.

3.3. Effect of the microenvironment, such as the polarity, viscosity, and pH, on the spectroscopic properties of THYQ

The microenvironment in the cavity of HSA and in viscous aqueous medium (Lysosome, Mitochondria of cells) have a contrasting difference between low polarity in the HSA cavity and high polarity in a viscous aqueous medium. To validate the effect of polarity of the medium on the fluorescence colour of **THYQ**, solutions of **THYQ** (10 μM) were made in solvents of varied polarity (Table S1[†]) with E_T^{30} values changing from 30.9 to 55.4, and their UV-vis and fluorescence spectra were recorded. **THYQ** in non-polar solvents with an E_T^{30} value ranging from 30.9 to 42.2 displayed an absorbance band at 420 nm. In DMSO, CH₃CN, and ethanol, as solvents with a higher E_T^{30} value, **THYQ** displayed an additional low-energy absorbance band at $530 \pm 2\text{ nm}$, probably due to a strong stabilization of the ground state (Fig. 1D). The fluorescence spectra of these solutions (λ_{ex} 420 nm) exhibited strong positive solvatochromism with a red-shift in the emission maximum with the increase in polarity (E_T^{30} value) (Fig. 1E) and a change in the fluorescence colour from blue in cyclohexane to yellow-orange in ethanol (Fig. 1J). Significantly, the plot of the E_T^{30} values of these solvents against their maximum emission wavelengths showed a linear relationship, with a slope of $7.89\text{ nm}/E_T^{30}\text{ unit}$ (Fig. 1F). Such a steep change in the wavelength of the emission maximum with an increase in E_T^{30} value is less known (Table S2[†]).

The UV-vis and fluorescence spectra of **THYQ** in binary mixtures of toluene and THF further validated the sensitivity of the probe to the polarity of the medium. In most of the fractions of toluene-THF (10–90%), there was only a small change in absorbance, but upon increasing the fraction of THF from 90% to 99.9%, the absorbance decreased from 0.211 to 0.177 (Fig. 1G). The emission spectrum of **THYQ** in THF displayed a maximum at 572 nm, the emission maximum of the HSA-**THYQ** complex. Upon steadily increasing the amount of toluene, the fluorescence intensity gradually decreased and the emission maximum gradually shifted from 572 to 527 nm (Fig. 1H and I) and the fluorescence colour of the solutions changed from green to yellow (Fig. 1K). Therefore, this resulted in a small range of E_T^{30} values, for THF (E_T^{30} 37.4) to toluene (E_T^{30} 33.9), and showed the viability of the probe even in a narrow range.²⁸



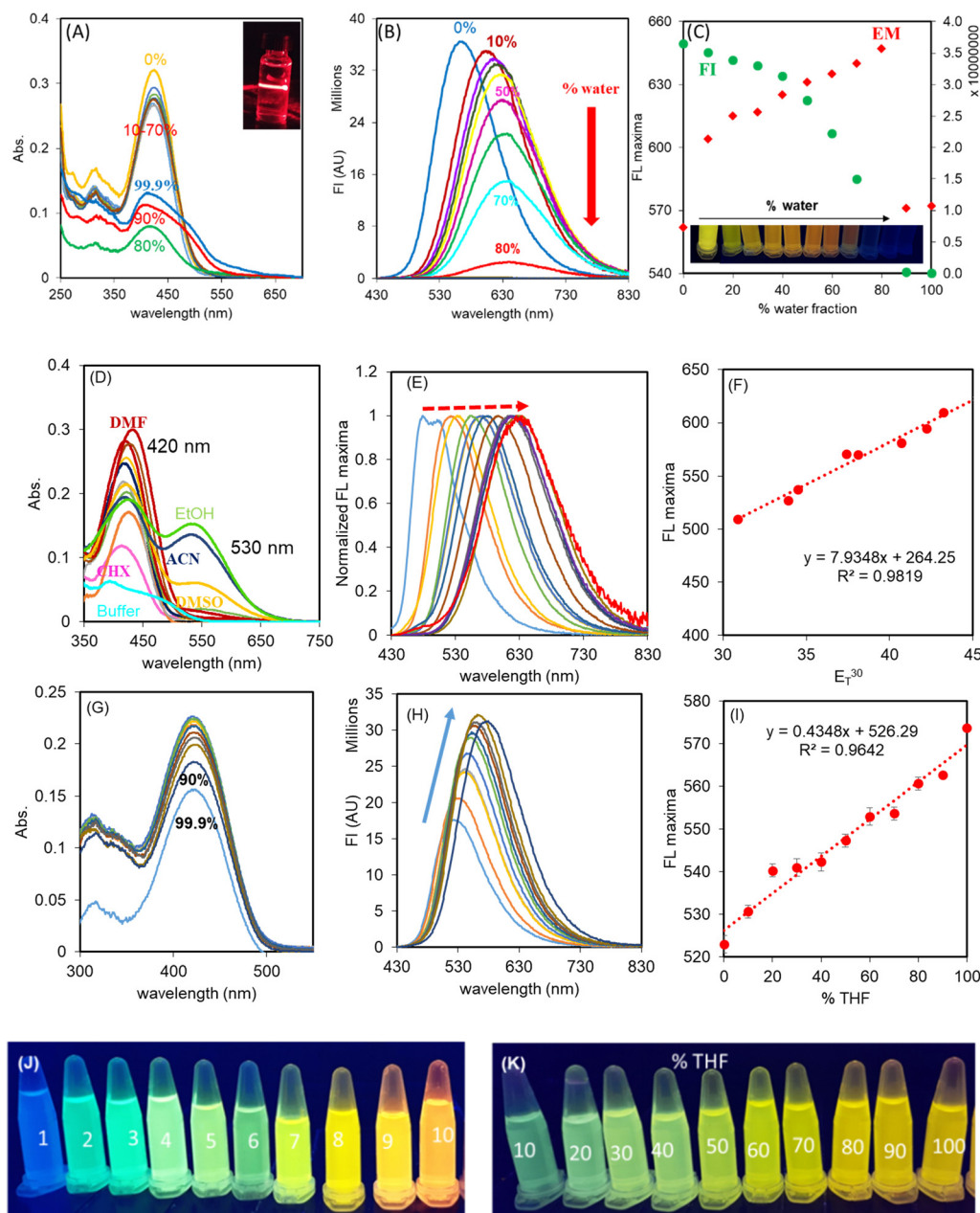
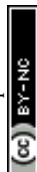


Fig. 1 (A) Absorption spectra of **THYQ** (10 μM) in THF-HEPES buffer binary mixtures, inset shows the Tyndall effect in the solution of **THYQ** in 99.9% HEPES buffer, representing the aggregation; (B) emission spectra of **THYQ** solutions in THF-buffer binary mixtures; (C) plot of f_w vs. the emission intensity and the maxima for the solutions of **THYQ**. Inset shows the change in emission colours with increasing f_w in THF; (D) absorption spectra and (E) normalized emission spectra of **THYQ** in organic solvents with increasing polarity (E_T^{30} value); (F) linear relationship between the emission wavelength at the maximum and E_T^{30} values; (G) absorption spectra and (H) emission spectra of **THYQ** in THF-toluene binary mixtures; (I) linear relationship between the emission wavelength at maxima and the fraction of THF in toluene. [**THYQ**] = 10 μM, λ_{ex} 420 nm; (J) fluorescence colours of **THYQ** solutions in various solvents under illumination at 365 nm: 1. cyclohexane, 2. toluene, 3. ether, 4. THF, 5. ethyl acetate, 6. acetone, 7. DMF, 8. DMSO, 9. CH₃CN, 10. ethanol; (K) fluorescence colours of **THYQ** in THF-toluene binary mixtures under illumination at 365 nm.

The fluorescence intensity (FI) of **THYQ** (at 572 nm) in water-glycerol binary mixtures at up to 50% of glycerol increased only by 1.6 times without any shift in emission maximum, but further increase with the amount of glycerol, especially in 80% and 90% glycerol solutions, where the fluorescence intensity increased sharply. In the 90% glycerol-water mixture, the FI increased by 18 times in

comparison to that in water and the fluorescence maximum was shifted from 572 nm to 640 nm (Fig. S6†). The restriction in rotation (RIR) at higher viscosity led to the increase in fluorescence.²⁹ Further, between pH 5–11, both the UV-vis and fluorescence spectra of **THYQ** remained stable, indicating its potential use under physiological conditions (Fig. S7†).



3.4. Selectivity and sensitivity of THYQ towards HSA

The probe **THYQ** upon moving into the cavity of a protein, a hydrophobic environment, could be expected to cause an enhancement in its fluorescence intensity and display a blue-shift in its emission maximum compared to that observed in water. In order to evaluate the selectivity and sensitivity of **THYQ** towards HSA in comparison to different biomolecules, 5 equivalents each of these were added to **THYQ** (10 μM , HEPES buffer, pH 7.4) and the fluorescence spectra of these solutions were recorded. It was noticed that the presence of HSA caused a 55-fold increase in the fluorescence intensity at 555 nm, whereas the addition of other biomolecules, like proteins, amino acids, anions, thiols, *etc.*, caused practically no change in fluorescence (Fig. 2A and S8†). Thus, the emission of **THYQ** in the presence of HSA (555 nm, green) and glycerol (640 nm, red) differentiated the two situations (Fig. 2B). In addition to this, the presence of HSA in solution could be distinctly differentiated without interference from any cations, anions, thiols, amines, or amino acids (Fig. S9†).

THYQ (10 μM , HEPES buffer, 0.1% THF) upon excitation at 420 nm displayed weak fluorescence with a maximum at 570 nm. The fluorescence intensity of **THYQ** upon the

addition of 50 μM HSA achieved a plateau within 5 min, indicating its rapid response towards HSA (Fig. 2C). The gradual addition of aliquots of HSA to **THYQ** led to a steady increase in emission intensity with the maximum at 555 nm. After the addition of 50 μM HSA, only a residual change in fluorescence intensity was observed. However, the UV-vis spectrum of **THYQ** showed only a small change upon the addition of HSA (Fig. S13†). The plot of $[\text{HSA}]$ vs. the fluorescence intensity showed a linear change between 0 to 0.13 μM HSA. The LOD for HSA was 2.8 nM as per IUPAC norms (Fig. 2D and E). Since, in human serum, the $[\text{HSA}]$ is 500–700 μM , we were interested in knowing the binding stoichiometry of **THYQ** (10 μM) with HSA under these conditions. Here, multivariate global regression analysis of the spectra for the titration of **THYQ** with HSA showed that at $[\text{HSA}] \geq 200 \mu\text{M}$, one molecule of **THYQ** binds with two molecules of HSA to form the **THYQ** $\cap(\text{HSA})_2$ complex with $\log\beta$ 9.52 and no formation of any other species at this concentration of HSA was observed. Significantly, at $[\text{HSA}] < 20 \mu\text{M}$, the $(\text{THYQ})_2\text{HSA}$ complex was the major species (Fig. S10A†).

Therefore, **THYQ** in buffer existed as aggregates, which may be in equilibrium with its monomers. Upon interaction with HSA, the monomers bind in the cavity of HSA to give a

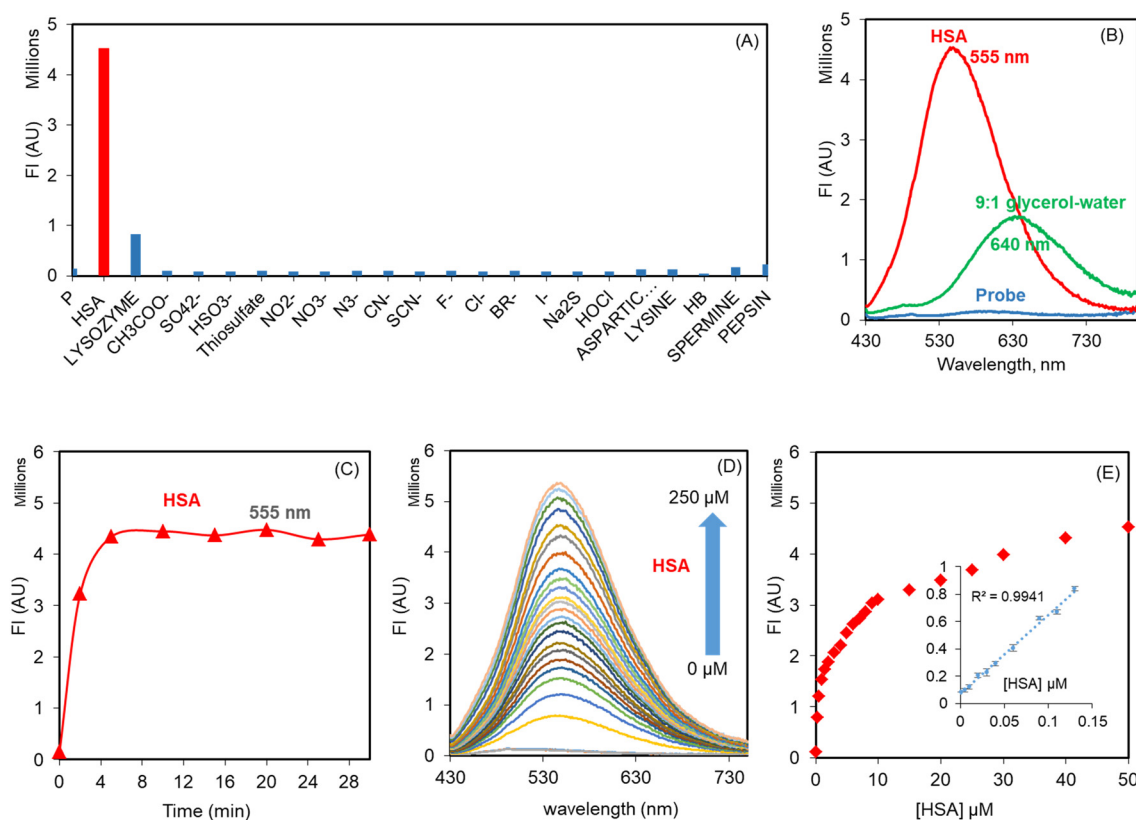


Fig. 2 (A) Change in fluorescence intensity of **THYQ** (10 μM , HEPES buffer, pH 7.4) with 5 equivalents each of HSA, anions, thiols, amines, and amino acids; (B) fluorescence spectra of **THYQ** upon the addition of HSA and glycerol; (C) time-dependent change in fluorescence upon the addition of 30 μM HSA to **THYQ** (10 μM , HEPES buffer, 0.1% THF); (D) fluorescence spectra of **THYQ** (10 μM) with the incremental addition of HSA; (E) plot of the fluorescence intensity vs. $[\text{HSA}]$ at 555 nm; inset shows the linear range and LOD for HSA, where I_0 and I are the fluorescence intensities of **THYQ** in the absence and presence of different amounts of HSA.



high fluorescence and the equilibrium is shifted towards the monomers. The high fluorescence could be attributed to the decreased polarity in the cavity of HSA and the restriction in rotation.³⁰ The participation of a FRET mechanism was negligible (Fig. S14†) as the UV-vis spectrum of HSA had a poor overlap with the fluorescence of **THYQ**.

3.5. Mechanism of interaction of **THYQ** with HSA

3.5.1. Binding site prediction of **THYQ in HSA.** In order to rationalize the effect of different drugs on the displacement of **THYQ** in the cavity of HSA and to find the binding site of **THYQ** in HSA, the solution **THYQ**–HSA (10:200) was titrated with warfarin, ibuprofen, bilirubin, and hemin. Quite interestingly, with 100 μM bilirubin/hemin (both subdomain IB specific), the fluorescence intensity of the **THYQ**–HSA complex was completely quenched. However, warfarin (subdomain IIA specific) and ibuprofen (subdomain IIIA specific) did not cause any substantial change in the fluorescence intensity of the **THYQ**–HSA complex (Fig. 3A). Therefore, in the **THYQ**–HSA complex, **THYQ** binds at the bilirubin site only and was displaced upon the addition of bilirubin and hemin only. The $\log\beta$ value for this displacement process is $\log\beta = 4.83 \pm 0.12$.

3.5.2. Circular dichroism studies. Circular dichroism (CD) experiments were performed to investigate the effect of **THYQ** on the secondary structure of HSA. The far UV spectral region of HSA (0.1 μM) displayed two characteristic dichroic bands at 208 and 222 nm, which indicate the feature of the α -helical structure of the protein. The addition of **THYQ** to HSA resulted in a decrease in the CD signal with no observable change in the signal wavelengths at 208 and 222 nm, suggesting only a small change in the α -helix content in HSA. The α -helicity value of free HSA was ~ 70.15 and decreased to ~ 65.60 in the presence of **THYQ** (1 equiv.), demonstrating that the secondary structure of HSA was not significantly affected by **THYQ** (Fig. 3B).

3.5.3. Dynamic light scattering (DLS) studies. DLS studies can provide insights into the aggregation behaviour of **THYQ**

in water and the changes in its size upon the addition of HSA, which can help indicate the mechanism of interaction of **THYQ** with HSA. The DLS of **THYQ** (10 μM , 0.1% THF) revealed the presence of aggregates with an average hydrodynamic diameter of 691 nm (Fig. 3C). Upon the addition of HSA (200 μM), the aggregates of **THYQ** completely disappeared and only particles with an average hydrodynamic diameter of 7 nm could then be observed (Fig. 3D). The further addition of HSA did not lead to any further changes in the sizes of the particles. These particles could be assigned to globular HSA molecules, which encapsulated the **THYQ** molecules. Therefore, in agreement with the proposed mechanism, the aggregates and monomers of **THYQ** remained in equilibrium, and the monomers upon moving in to the cavity of HSA exhibited only the presence of HSA in the DLS experiments. The DLS experiments further revealed that the presence of BR resulted in an aggregation of HSA, but upon the addition of **THYQ**, they reverted back to non-aggregated HSA molecules (Fig. S10†), but this did not affect the fluorescence at 430–630 nm and so the detection of BR.

3.5.4. Effect of **THYQ on the fluorescence of HSA.** The binding of the probe **THYQ** in the cavity of HSA was further investigated by titrating HSA with **THYQ**. HSA (λ_{ex} 290 nm) displayed emission with a maximum at 345 nm. The gradual addition of **THYQ** to HSA (10 μM) resulted in a systematic quenching of the fluorescence intensity of HSA at 345 nm, and with 150 μM **THYQ**, >95% of the original fluorescence intensity was quenched. Careful analysis of these spectra showed that **THYQ** led to a blue-shift in the emission maximum of HSA by ~ 10 nm from 345 nm to 335 nm (Fig. S11B†). Multivariate global analysis of these data showed that one HSA molecule can encapsulate two **THYQ** molecules (Fig. S11C†), which was in concordance with the titration of **THYQ** with HSA and recording the fluorescence at 555 nm.

Thus, all these studies revealed that **THYQ** in the presence of excess (>200 μM) HSA preferably binds at subdomain 1B of HSA – the binding domain of bilirubin. **THYQ** exhibited

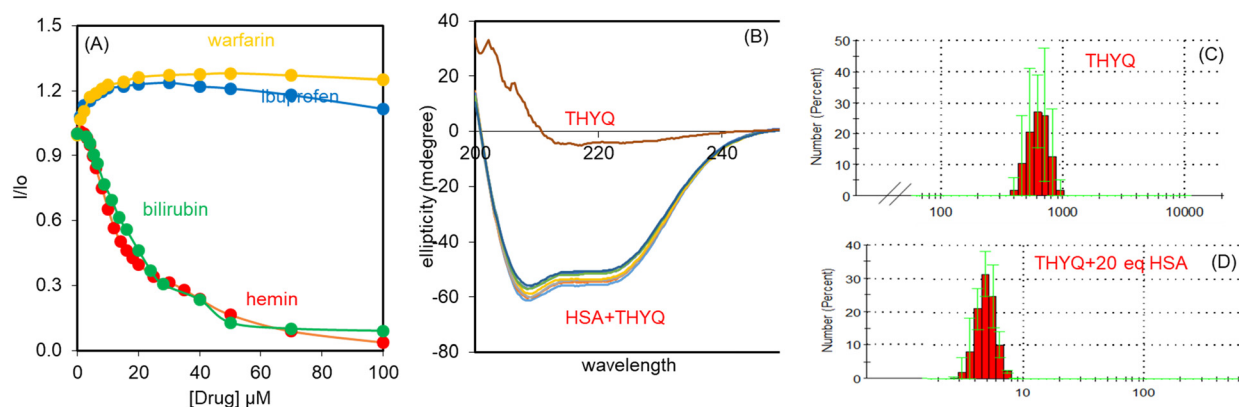


Fig. 3 (A) Effect of the increasing concentrations of site markers on the fluorescence of **THYQ**–HSA (10:200) complex; (B) CD spectra of HSA with an increasing amount of **THYQ**; (C and D) DLS of (C) **THYQ** and (D) **THYQ** + 200 μM HSA.



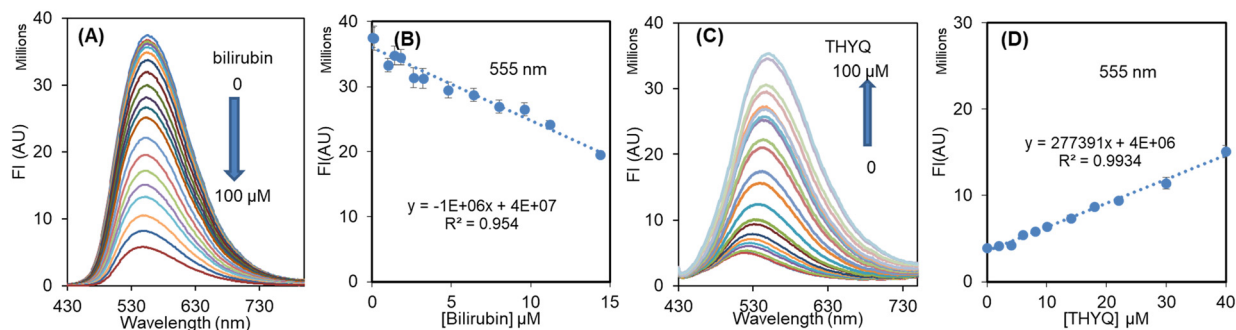


Fig. 4 (A) Change in fluorescence spectrum of THYQ-HSA (10:200) with increasing the concentration of bilirubin; (B) linear plot showing the decrease in fluorescence intensity at 555 nm with [bilirubin]; (C) change in fluorescence spectrum of BR-HSA (20:200) complex with [THYQ]; (D) linear plot showing the increase in fluorescence intensity at 555 nm with [THYQ].

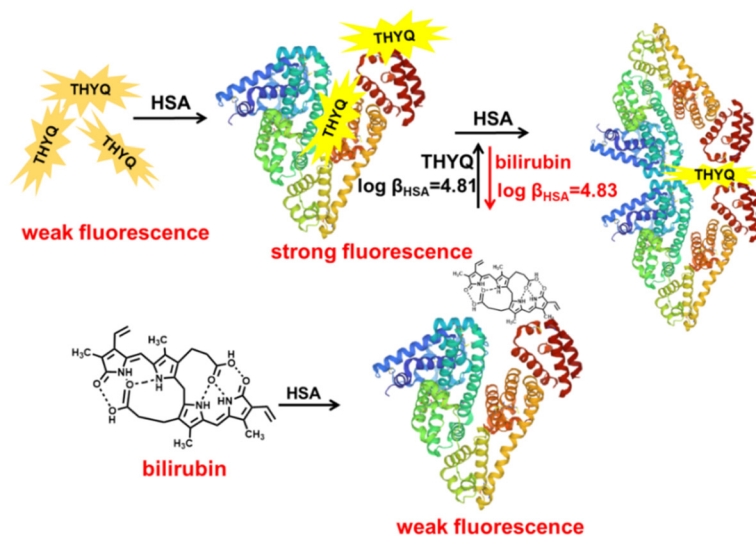
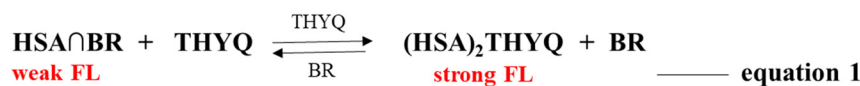
differential changes in fluorescence with HSA, and with the viscosity and polarity of the medium, and has potential for the development of a strategy for the detection of bilirubin.

4. Protocol for the determination of bilirubin in HSA

The preceding results showed that in the THYQ-HSA (1:20) complex the addition of bilirubin resulted in an efficient quenching of fluorescence, *i.e.* bilirubin was able to displace the THYQ molecule from the THYQ-(HSA)₂ complex (Fig. 4A and B). For the displacement of THYQ, the $\log \beta$ value was 4.83 ± 0.12 . We envisaged that if the fluorescence probe THYQ would be able to displace the bilirubin from the cavity of HSA, the equilibrium state between the complexes of HSA with THYQ and bilirubin would be validated (eqn

1, Scheme 2). The addition of THYQ to the weakly fluorescent bilirubin-HSA (1:20) displaced bilirubin with THYQ to form a fluorescent complex (Fig. 4C and D). The $\log \beta$ value was 4.81 ± 0.13 . It was noteworthy that the addition of bilirubin to THYQ or HSA alone did not lead to any significant change in fluorescence intensity under these conditions. This provides a method for the detection of BR from the HSA-BR mixture. Further, proteins, like pepsin, lysozyme, and bromoaniline, did not interfere in detection of BR (Fig. S12†).

The normal level of HSA in human serum is in the range of $35\text{--}50\text{ g L}^{-1}$ or approx. $500\text{--}700\text{ }\mu\text{M}$. Therefore, keeping the $[\text{HSA}] = 500\text{ }\mu\text{M}$, different concentrations of bilirubin, *i.e.* 0, 20, 40, 60, 80, 200, and $300\text{ }\mu\text{M}$, were added and these solutions were titrated with THYQ. As expected, it was found that as the concentration of BR increased in HSA, it required a greater and greater amount of THYQ to displace it. This



Scheme 2 Schematic presentation of the reversible displacement of THYQ by bilirubin and vice versa from its respective complex with HSAs.



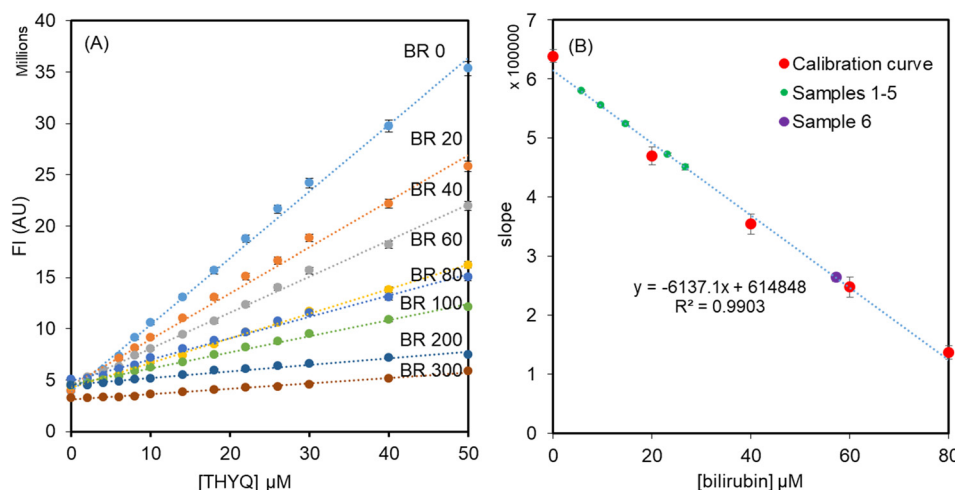


Fig. 5 (A) Titration of solutions of HSA (500 μM) + bilirubin (0–300 μM) with the probe THYQ; (B) linear relationship between the slopes and [bilirubin].

resulted in a decrease in the slope of the linear plot of the fluorescence intensity vs. [THYQ]. Consequently, the slope for the titration of the BR–HSA complex was linearly dependent on the [BR] in Fig. 5A. The plot of the slope of these linear plots vs. [bilirubin] (Fig. 5B) revealed that the value of the slope changed linearly between 0–80 μM [bilirubin], and thus may have application potential in determining bilirubin from human serum.

5. Analysis of bilirubin in clinical samples

Further to validate the practical application of the fluorescent probe THYQ, the detection of bilirubin levels was performed in human blood serum samples. For samples 1–5, 400 μL human serum was diluted with 400 μL of HSA (500 μM , 0.01 M HEPES buffer). The fluorescence spectrum of the solution was recorded and then aliquots of THYQ (8 μL , 10 μM) were added twice and each time the fluorescence spectrum of the solution was recorded. The plot of the fluorescence intensity vs. [THYQ] was linear, for which the slope was calculated. The [bilirubin] was calculated from the calibration curve as in Fig. 5B and then multiplied by 2 to compensate for the dilution factor, before finally being converted to mg dL^{-1} (Table 1). For serum sample 6, with a higher amount of

bilirubin (as apparent from the dark yellow colour), 200 μL serum sample was diluted with HSA (600 μL , 500 μM , 0.01 M HEPES buffer) to four times its volume and the slope for titration was determined by adding two aliquots of THYQ. The [bilirubin] was calculated from the calibration curve and then multiplied by 4 to compensate for the dilution factor. The amount of bilirubin determined by this fluorescence method was within $\pm 10\%$ of that determined by a clinical method.

Therefore, the present fluorescence-based quantification of bilirubin is unique in that does not involve any chemical reaction and primarily depends on the displacement of bilirubin in HSA–BR complex by THYQ to cause fluorescence “Turn ON” under physiological conditions and straightforwardly determines BR from serum. This approach enables the real-time determination of bilirubin without harming any of the substrate,²⁰ which is not achieved by the chemosensors discussed below.

The fluorescent probes reported earlier for the detection of bilirubin (BR) were based on organic molecules and nanomaterials and most of them show “Turn OFF” processes (Table S3,† ref. 1, 4–7 and 10–13). Even, the fluorescent systems showing “Turn ON” processes have a number of limitations. The nanomaterials with “Turn ON” mechanism towards BR are active only under strong acidic (pH 2.5, 5.0) (Table S3,† ref. 8 and 14) and basic (pH 11.4) (Table S3,† ref. 9) conditions and depend on the release of fluorescence upon the coordination of BR with Fe^{3+} . Moreover, BR is detected through spiking methods and does not represent a clinical detection. In the case of “Turn ON” fluorescent organic molecular systems^{16,17} (Table S3,† ref. 2 and 3), the redox reaction of Fe^{3+} (added in excess) with free bilirubin produces Fe^{2+} , which causes deoxygenation of the probe *N*-oxide to release the fluorescence. The two mechanisms are contradictory to each other in terms of the respective coordination and oxidation of BR with Fe^{3+} in nanomaterials and organic systems.

Table 1 Comparison of [bilirubin] (mg dL^{-1}) by using THYQ as a probe and its comparison with clinical results

Sample no.	Diazo method (mg dL^{-1})	Present method (mg dL^{-1})	% recovery
1	0.7	0.66 ± 0.02	95 ± 3
2	1.2	1.12 ± 0.03	94 ± 3
3	1.9	1.71 ± 0.05	90 ± 2
4	2.9	2.71 ± 0.05	93 ± 2
5	3.2	3.12 ± 0.10	97 ± 3
6	12.6	13.37 ± 0.25	106 ± 2



6. Conclusions

THYQ was found to bind selectively at subdomain IB of HSA and exhibited a 55-fold increase in fluorescence intensity at 555 nm and an LOD for HSA of 2.8 nM. The reversible displacement of **THYQ** in **THYQ**–HSA complex with bilirubin ($\log \beta_{\text{HSA}} = 4.83 \pm 0.12$) and that of BR in the non-fluorescent BR/HSA complex with **THYQ** ($\log \beta_{\text{HSA}} = 4.81 \pm 0.13$) provides an opportunity for the detection of bilirubin from human serum through a displacement approach, with an LOD for BR of 0.004 mg dL⁻¹ (68 nM). The slope of titration of BR–HSA with **THYQ** was found to be linearly dependent on [bilirubin] in HSA and enables a fluorescence-based direct method for the detection of bilirubin below normal (0.7 mg dL⁻¹, 12 µM) to hyperbilirubinemia conditions (12.6 mg dL⁻¹, 216 µM). The results for the detection of BR by this displacement approach in real samples were in good agreement with clinical findings.

Human sample statement

The permission for the experiments with blood samples was provided by the institutional ethical committee, Guru Nanak Dev University, and in accordance with the Declaration of Helsinki. Informed consents were obtained from all participants in this study.

Author contributions

The manuscript was written through contributions of all authors. All authors have given approval to the final version of the manuscript.

Conflicts of interest

There are no conflicts to declare.

Acknowledgements

SK thanks UGC, New Delhi for UGC-BSR faculty fellowship F.4-5(11)/2019 (BSR). We also thank UGC for PURSE, UPE and CAS programs and DST for FIST program.

References

- 1 T. Slusher, T. Zamora, D. Appiah, J. Stanke, M. Strand, B. Lee, S. Richardson, E. Keating, A. Siddappa and B. Olusanya, *BMJ Paediatr. Open*, 2017, **1**, 000105.
- 2 R. P. Wennberg, *Clin. Chem.*, 2012, **58**, 811–813.
- 3 S. Ullah, K. Rahman and M. Hedayati, *Iran. J. Public Health*, 2016, **45**, 558–568.
- 4 A. A. H. Van den Bergh and P. Mueller, Bilirubin, *Biochem. Z.*, 1916, **77**, 90–103.
- 5 A. Westwood, *Ann. Clin. Biochem.*, 1991, **28**, 119–130.
- 6 R. R. Anjana, J. S. Anjali Devi, M. Jayasree, R. S. Aparna, B. Aswathy, G. L. Praveen, G. M. Lekha and G. Sony, *Microchim. Acta*, 2018, **185**, 1–11.
- 7 K. Abha, J. Nebu, J. S. A. Devi, R. S. Aparna, R. R. Anjana, A. O. Aswathy and S. George, *Sens. Actuators, B*, 2019, **282**, 300–308.
- 8 B. Barik and S. Mohapatra, *Anal. Biochem.*, 2022, **654**, 114813.
- 9 W. Xiao, J. Liu, Y. Xiong, Y. Li and H. Li, *Anal. Bioanal. Chem.*, 2021, **413**, 7009–7019.
- 10 K. Yi, H. Li, X. Zhang and L. Zhang, *Inorg. Chem.*, 2021, **60**, 3172–3180.
- 11 C. Xia, Y. Xu, M.-M. Cao, Y.-P. Liu, J.-F. Xia, D.-Y. Jiang, G.-H. Zhou, R.-J. Xie, D.-F. Zhang and H.-L. Li, *Talanta*, 2020, **212**, 120795.
- 12 S. Ellairaja, K. Shenbagavalli, S. Ponmariappan and V. S. Vasantha, *Biosens. Bioelectron.*, 2017, **91**, 82–88.
- 13 V. Srinivasan, M. A. Jhonsi, N. Dhenadhayalan, K.-C. Lin, D. A. Ananth, T. Sivasudha, R. Narayanaswamy and A. Kathiravan, *Spectrochim. Acta*, 2019, **221**, 117150.
- 14 Y. Hisamatsu, K. Otani, H. Takase, N. Umezawa and T. Higuchi, *Chem. – Eur. J.*, 2021, **27**, 6489–6499.
- 15 S. Qi, X. He, S. Zhang, P. Xu, M. Su, B. Dong and B. Song, *Anal. Chim. Acta*, 2023, **1238**, 340657.
- 16 E. Ahmmed, A. Mondal, A. Sarkar, S. Chakraborty, S. Lohar, N. C. Saha, K. Dhara and P. Chattopadhyay, *ACS Appl. Bio Mater.*, 2020, **3**, 4074–4080.
- 17 E. Ahmmed, A. Mondal, N. C. Saha, K. Dhara and P. Chattopadhyay, *Anal. Methods*, 2021, **13**, 5651–5659.
- 18 C. E. Petersen, C.-E. Ha, K. Harohalli, J. B. Feix and N. V. Bhagavan, *J. Biol. Chem.*, 2000, **275**, 20985–20995.
- 19 G. H. Beaven, A. D'Albis and W. B. Gratzer, *Eur. J. Biochem.*, 1973, **33**, 500–509.
- 20 (a) A. C. Sedgwick, J. T. Brewster II, T. Wu, X. Feng, S. D. Bull, X. Qian, J. L. Sessler, T. D. James, E. V. Anslyn and X. Sun, *Chem. Soc. Rev.*, 2021, **50**, 9–38; (b) B. T. Nguyen and E. V. Anslyn, *Coord. Chem. Rev.*, 2006, **250**, 3118–3127.
- 21 S. Dhiman, R. Kour, G. Kumar, S. Kaur, V. Luxami, P. Singh and S. Kumar, *Mater. Chem. Front.*, 2022, **6**, 2651–2660.
- 22 J. Mocak, A. M. Bond, S. Mitchell and G. Scollary, *Pure Appl. Chem.*, 1997, **69**, 297–328.
- 23 G. A. Crosby and J. N. Demas, *J. Phys. Chem.*, 1971, **75**, 991–1024.
- 24 H. Gampp, M. Maeder, C. J. Meyer and A. D. Zuberbühler, *Talanta*, 1985, **32**, 257–264.
- 25 M. Sasmal, A. S. M. Islam, R. Bhowmick, D. Maiti, A. Dutta and M. Ali, *ACS Appl. Bio Mater.*, 2019, **2**, 3551–3561.
- 26 (a) F. C. Spano, *Acc. Chem. Res.*, 2010, **43**, 429; (b) E. C. Kwok, D. P. Tsang, M. Chan and V. W. Yam, *Chem. – Eur. J.*, 2013, **19**, 2757–2767; (c) N. J. Hestand and F. C. Spano, *Chem. Rev.*, 2018, **118**, 7069–7163.
- 27 H. Xiao, P. Li and B. Tang, *Coord. Chem. Rev.*, 2021, **427**, 213582; Z. Zhang, Z. Gou, B. Dong and M. Tian, *Sens. Actuators, B*, 2022, **355**, 131349; C. Wu, X. Li, T. Zhu, M. Zhao, Z. Song, S. Li, G. Shan and G. Niu, *Anal. Chem.*, 2022, **94**, 3881–3887.
- 28 (a) K. Kudo, A. Momotake, Y. Kanna, Y. Nishimura and T. Arai, *Chem. Commun.*, 2011, **47**, 3867–3869; (b) J. Yin, M. Peng, Y. Ma, R. Guo and W. Lin, *Chem. Commun.*, 2018, **54**,



- 12093–12096; (c) R. Chen, Z. Li, C. Peng, L. Wen, L. Xiao and Y. Li, *Anal. Chem.*, 2019, **91**, 1928–1935.
- 29 (a) R. D. Telore, M. A. Satam and N. Sekar, *Dyes Pigm.*, 2015, **122**, 359–367; (b) H. S. Kumbhar, S. S. Deshpande and G. S. Shankarling, *ChemistrySelect*, 2016, **1**, 2058–2064.
- 30 (a) S. Dhiman, R. K. G. Kumar, S. Kaur, V. Luaxmi, P. Singh and S. Kumar, *Mater. Chem. Front.*, 2022, **6**, 2651–2660; (b) S. Samanta, S. Halder and G. Das, *Anal. Chem.*, 2018, **90**, 7561–7568; (c) S. I. Reja, I. A. Khan, V. Bhalla and M. Kumar, *Chem. Commun.*, 2016, **52**, 1182–1185.

